Target-specific mechanics of phagocytosis: protrusive neutrophil response to zymosan differs from the uptake of antibody-tagged pathogens

Cheng-Yuk Lee[1,2], Marc Herant[3] and Volkmar Heinrich[1,*]

[1]Department of Biomedical Engineering, University of California Davis, Davis, CA 95616, USA
[2]Department of Chemical Engineering and Materials Science, University of California Davis, Davis, CA 95616, USA
[3]Department of Biomedical Engineering, Boston University, Boston, MA 02215, USA
*Author for correspondence (vheinrich@ucdavis.edu)

Accepted 22 November 2010
Journal of Cell Science 124, 1106-1114

doi:10.1242/jcs.078592

Summary

The physical mechanisms that control target-specific responses of human neutrophils to distinct immune threats are poorly understood. Using dual-micropipette manipulation, we have quantified and compared the time courses of neutrophil phagocytosis of two different targets: zymosan (a prominent model of fungal infection), and antibody-coated (Fc) particles. Our single-live-cell/single-target approach exposes surprising differences between these two forms of phagocytosis. Unlike the efficient uptake of 3-μm Fc targets (within ~66 seconds), the engulfment of similarly sized zymosan is slow (~167 seconds), mainly due to the formation of a characteristic pedestal that initially pushes the particle outwards by ~1 μm. Despite a roughly twofold difference in maximum cortical tensions, the top 'pull-in' speeds of zymosan and Fc targets are indistinguishable at ~33 nm/second. Drug inhibition shows that both actin as well as myosin II partake in the regulation of neutrophil cortical tension and cytoplasmic viscosity; other than that, myosin II appears to play a minor role in both forms of phagocytosis. Remarkably, an intact actin cytoskeleton is required to suppress, in antibody-mediated phagocytosis, the initially protrusive deformation that distinguishes the neutrophil response to zymosan.

Key words: Biomechanics, Cell motility, Immune recognition, Immunophysics, Micropipette manipulation, Single-cell assay

Introduction

Cells that perform controlled, directional movements have piqued the curiosity of scientists for centuries. In particular, the motile foot soldiers of the immune system (neutrophils, monocytes and macrophages) have attracted special, cross-disciplinary interest. Vital among their functions are immune processes like phagocytosis and chemotaxis that depend on two inextricable, complementary parts: the timely recognition of pathogens, and the aptitude of cells to change their shape and perform mechanical work. Biological research primarily addresses the former, dedicating great efforts to mapping the reaction networks of signaling biochemistry involved in the detection, uptake, and processing of phagocytic targets (Dewitt and Hallett, 2002; Janeway and Medzhitov, 2002; Kobayashi et al., 2002; Medzhitov and Janeway, 2002; Underhill and Ozinsky, 2002; Dormann et al., 2004; Swanson and Hoppe, 2004; Stuart and Ezekowitz, 2005; Swanson, 2008), as well as in chemotactic cell migration (Parent and Devreotes, 1999; Dormann et al., 2004; Janetopoulos et al., 2004). However, little is known about the fundamental physical mechanisms orchestrating the interplay between immune recognition and controlled cellular motion. Open questions relate, for example, to the conversion of biochemical signals into mechanical forces, or the coordination of different forces to achieve a particular cellular deformation. Clearly, a comprehensive understanding of the cause–effect complexity of the behavior of motile immune cells requires an interdisciplinary perspective (Herant et al., 2005; Touret et al., 2005; Araki, 2006; Herant et al., 2006; Hallett and Dewitt, 2007; Holt et al., 2007; Huynh et al., 2007; Hallett et al., 2008; Kay et al., 2008; Fletcher and Mullins, 2010).

Bridging immunology and mechanics, this study addresses the hypothesis that distinct target-specific forms of phagocytosis might involve qualitatively different physical mechanisms of cell deformation. We test this hypothesis using our recently developed biophysical technique based on dual-micropipette manipulation (Fig. 1A) (Heinrich and Rawicz, 2005; Herant et al., 2005). This technique enables us to select initially passive cells and manoeuvre them into soft contact with chosen targets (Fig. 1B–F). Analysis of the ensuing target uptake allows us to quantify and compare the time courses of different forms of phagocytosis. Advantages of this approach over traditional bulk assays include: (1) Experiments are based on a single-cell/single-target assay using live cells. (2) Phagocytes are non-adherent and quiescent prior to contact with a target. (3) Contacts between cells and targets are well controlled. (4) An essentially axisymmetric configuration makes the experiments uniquely amenable to quantitative analysis. (5) The experiments provide the time courses of several key parameters of phagocytosis for each cell, such as the position and speed of the target, or the cortical tension (Herant et al., 2005) of the phagocyte. (6) Drug-inhibition experiments are not limited to binary outcomes, but instead reveal which stages of phagocytosis are affected more or less by each inhibitor. (7) The experimental results can be directly compared with computer simulations (Herant et al., 2006; Herant et al., 2011), which enables us to corroborate or discard hypotheses about the mechanoregulation of phagocytosis.

Using this quantitative approach, we examine phagocytosis in terms of five categories of mechanical effectors: adhesion, protrusion, contraction, tension, and viscosity. Stimulus-dependent variations in the interplay of these effectors produce a broad range

Journal of Cell Science

of vital, autonomous deformations. Even the seemingly well-defined process of phagocytosis exists in a number of different forms, depending on the cell and/or target type (Allen and Aderem, 1996; Herre et al., 2004). It was reported as early as 1977 that in complement-mediated phagocytosis by macrophages, the target appeared to 'sink' into the cell, whereas antibody-coated targets triggered the protrusion of pseudopods from the cell at the onset of engulfment (Kaplan, 1977). [This observation has recently come under dispute, however (Hall et al., 2006; Patel and Harrison, 2008).] Focusing here on the mechanics of early fungal recognition, we inspect the physical response of human neutrophils to zymosan, an insoluble, particulate fraction from yeast cell walls that has served as a model system in the study of fungal infection for many decades (Pillemer and Ecker, 1941; Di Carlo and Fiore, 1958). We assess the target specificity of this response by contrasting it with the phagocytosis of similarly sized antibody-coated targets (Fc beads).

Results

Distinct phagocytosis of zymosan and Fc beads

To ensure that all experiments started from a common baseline, we generally maintained the neutrophils in a quiescent state prior to exposure to phagocytic targets. We judged the cells' quiescence by their spherical shape, lack of interaction with the chamber bottom, and absence of spontaneous pseudopod formation (Fig. 1B). In each single-cell experiment, a passive neutrophil was selected and lifted above the chamber bottom with a micropipette [see Heinrich and Rawicz (Heinrich and Rawicz, 2005) for a tutorial on micropipette manipulation], eliminating interference from cell–substrate interactions of adherent, and thus inevitably pre-activated, immune cells. Another pipette was used to bring a zymosan particle or antibody-opsonized target bead (~3 μm diameter) into soft contact with the cell, usually resulting in immediate adhesion (Fig. 1C–F). After releasing the target, images of the ensuing phagocytosis were recorded to a computer hard disk for later analysis.

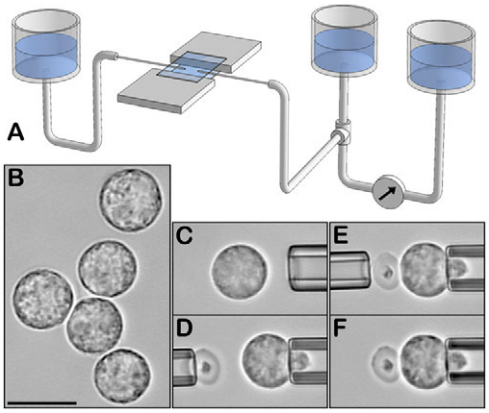

Fig. 1. Dual-micropipette setup for single-cell/single-target phagocytosis experiments. (**A**) The experiment chamber has two open sides for access by facing pipettes. The pipettes are connected to vertically movable water reservoirs. A properly zeroed reference reservoir (right) allows for accurate measurement of the aspiration pressure with a differential pressure transducer. (**B**) Isolated human neutrophils are maintained in a quiescent, non-adherent state. (**C**–**F**) A single cell is picked up with the right pipette at small suction. The left pipette is used to manoeuvre a target (here, a zymosan particle) into soft contact with the cell. Scale bar: 10 μm.

Fig. 2 reveals intriguing differences between the time-dependent morphologies of neutrophil phagocytosis of zymosan particles (Fig. 2A) and antibody-coated beads (Fig. 2B; see also supplementary material Movies 1 and 2). A distinguishing feature of the initial phase of zymosan engulfment is the protrusion of a transient cellular pedestal that effectively pushes the particle away from the main cell body. Thus, pseudopod growth commences in a direction that is normal to the cell-target contact region in this 'push-out' phase of zymosan phagocytosis, as illustrated also in the scanning-electron and confocal images in Fig. 3. By contrast, antibody-mediated phagocytosis begins with the formation of a pseudopodial lamella moving tangentially to the bead surface. Throughout the remaining course of engulfment, the pseudopod triggered by zymosan generally appears more irregular, and its motion less centered on the target, than the lamella surrounding an antibody-opsonized bead.

A comprehensive summary of our quantitative comparison of the two pathways is presented in Fig. 4. Fig. 4A,B depicts examples of positional traces of the two different targets. We measured such traces using custom-written software that allows us to track the target position relative to the (opposite side of the) cell body in recorded videomicrographs (illustrated in Fig. 5). The steepest slope of each trace is the maximum target speed (cf. Fig. 4C), which we determined as follows: Whenever the slope of the position-versus-time graph remained constant over a sizeable distance (~1.5–2 μm) during the period of fastest target motion, we fitted a straight line to this data range and identified the maximum speed with (the absolute value of) the slope of this line. This approach has been adequate for all zymosan traces, which frequently display constant-speed motion over distances as large as 2.5–3 μm. On the other hand, the traces of Fc beads generally

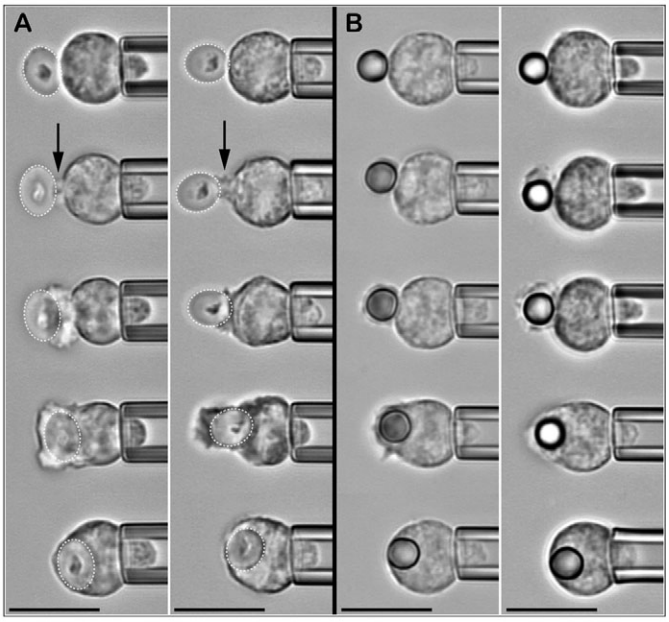

Fig. 2. Single-cell/single-target experiments reveal target-specific phagocytosis morphologies. (**A**) Two sequences of videomicrographs illustrate the typical timeline of neutrophil phagocytosis of zymosan. Arrows mark the distinct pedestal that pushes the zymosan particle (circled by white dotted line) away from the cell at the onset of phagocytosis. (**B**) Typical morphology of the phagocytosis of antibody-coated polystyrene beads. Scale bars: 10 μm.

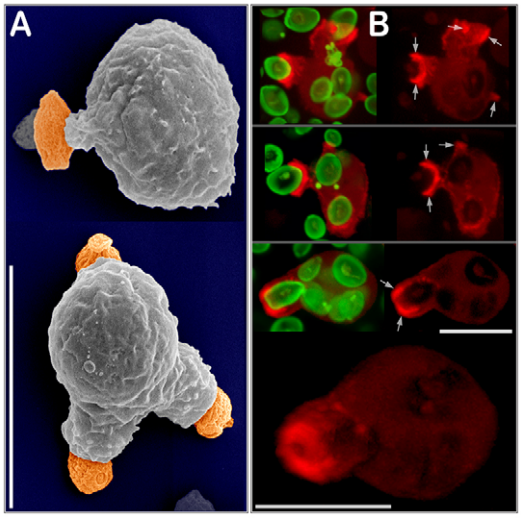

Fig. 3. Distinctive protrusive response to zymosan particles. (**A**) Pseudocolor SEM images of different stages of zymosan phagocytosis by human neutrophils. (**B**) Actin (labeled red) redistribution during protrusive phagocytosis of fluorescent zymosan (green) by human neutrophils. The top three rows show merged confocal images on the left and the red channel on the right. Arrows mark hotspots of high-density actin at sites of protrusion. The bottom panel depicts an enlarged 3D reconstruction of the red channel of the third cell (slightly rotated to expose the ring of high-density actin at the closing front of the pseudopod). Scale bars: 10 µm.

exhibit shorter linear segments, and in some cases their shape is sigmoidal, lacking a prominent linear range. In the latter cases, we used a sigmoidal fit to model the inward bead motion and identify the maximum speed with (the absolute value of) the slope at the inflection point.

Fig. 4A,B also includes graphs of the time-dependent cortical tension, i.e. the resistance of the neutrophil cortex to expansion of its surface area. Our micropipette-aspiration setup enabled us to monitor the cortical tension during phagocytosis in the following manner (Herant et al., 2005). Simple geometry dictates that a new cellular protrusion can only form if it is accompanied by an increase of the local cell-surface area. For a micropipette-held cell, the most efficient way to recruit surface area would be to retract the cell projection out of the pipette, thus simply re-shaping the cellular envelope without expanding its total area. We counteracted this tendency by continually adjusting the pipette-suction pressure in our experiments, maintaining a more or less constant cell-projection length inside the pipette. In this way, we can directly monitor the mechanical effort spent by the cell as it increases its total surface area. A well-known variant of Laplace's law relates the recorded aspiration pressure to the cell's cortical tension (see Materials and Methods) (Heinrich and Rawicz, 2005).

Overall, our analysis of curves such as shown in Fig. 4A,B focused on four quantities defined in Fig. 4C: the duration of target engulfment, the maximum push-out distance of the target, the maximum speed at which the target is moved into the cell, and the maximum tension measured during uptake of the target. The engulfment time (Fig. 4D) is the time elapsed between the first unambiguous sign of pseudopod formation (local to a newly adherent target) and the closure of the phagocytic cup. On average, zymosan phagocytosis (engulfment time ~167 seconds) takes about 2.5 times longer than the more efficient uptake of 3-µm Fc beads (~66 seconds). As evinced by the engulfment times of 5-µm (diameter) Fc beads included in Fig. 4D, the slower uptake of zymosan particles (which on average are slightly larger than the 3-µm beads) was not due to target-size-dependent variations of the timing of engulfment (Herant et al., 2006). Instead, considerable time is taken up by the initial push-out phase of zymosan.

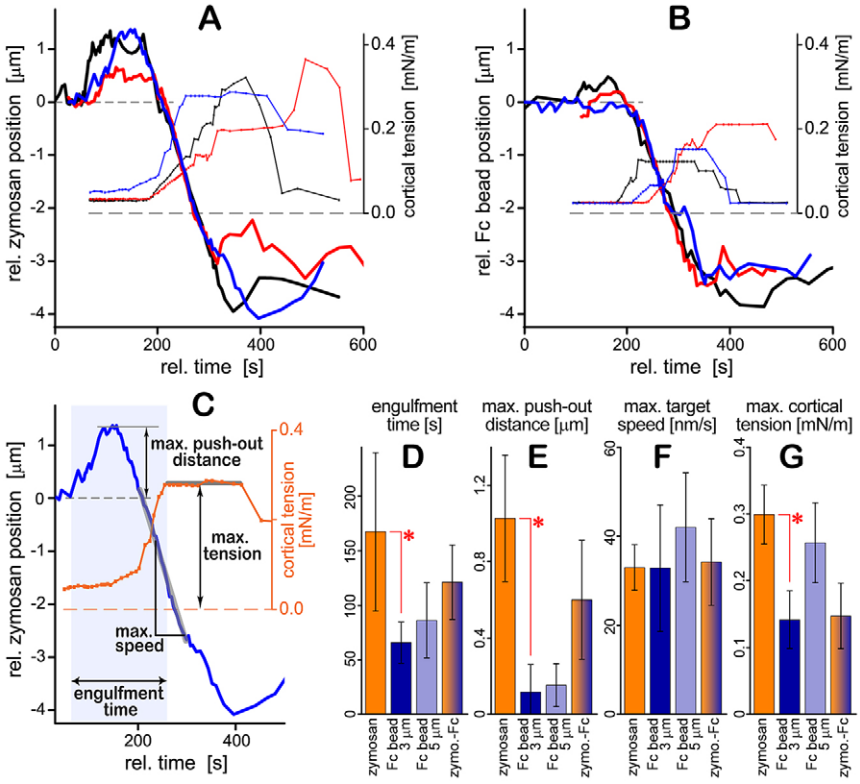

Fig. 4. Quantitative comparison of the phagocytosis of zymosan particles and antibody-coated targets (Fc beads with ~3 µm diameter). (**A**,**B**) Three positional traces of zymosan particles (A) and Fc beads (B) are shown together with the cortical tensions as functions of time. The individual time axes were aligned for maximum overlap during the inward movement of the target. (**C**) Illustration of our analysis of the target displacement and the cortical tension during phagocytosis. (**D–G**) Average engulfment time, maximum push-out distance, highest target speed and maximum cortical tension were measured in a total of n=74 single-cell phagocytosis experiments using the two different targets. Included are the respective values measured with larger (5 µm) beads (n=11). Also included are results obtained during the uptake of zymosan particles that had been coated with antibodies (zymo.-Fc; n=10; see also supplementary material Fig. S1). Error bars denote s.d., *P<0.01.

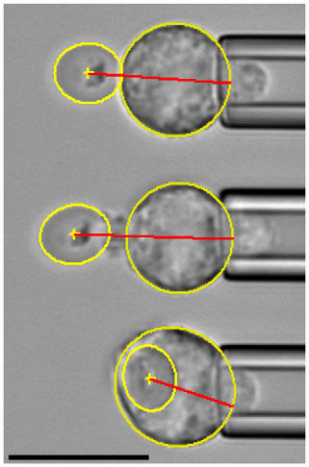

Fig. 5. Tracking of the target position relative to the cell body in suitable videomicrographs. Elliptical overlays (yellow) were positioned, sized and rotated to best match the outline of the target and the (opposite side of the) cell body, respectively. The distance between the target center and the back of the cell (denoted by the red line) was recorded. This approach allowed us to compensate for sideways movements of the target (i.e. off the axis defined by the pipette) as long as the target remained within the given focal plane of the microscope objective. Scale bar: 10 µm.

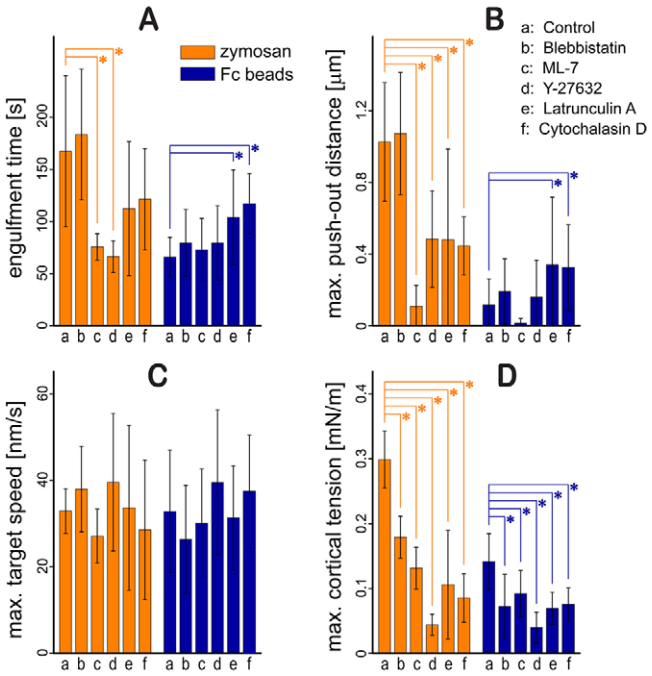

Fig. 6. Inhibitor effects on the four quantities used to compare phagocytosis of zymosan and Fc beads. (**A–D**) Average engulfment time (A), maximum push-out distance (B), maximum target speed (C) and maximum cortical tension (D) were measured in single-cell phagocytosis experiments using zymosan and Fc beads. The inhibitor concentrations were: 50 µM blebbistatin (b), 10 µM ML-7 (c), 10 µM Y-27632 (d), 3 nM latrunculin (e), and 500 nM cytochalasin D (f). Error bars denote s.d., **P*<0.01.

Confirming the qualitative observations shown in Fig. 2, the initial push-out distance of zymosan was consistently large (on average ~1.03 µm; Fig. 4E), whereas only half of the examined cells displaced antibody-coated targets outwards at all, and in such cases the displacements usually were much smaller (overall average ~0.12 µm).

Unlike the disparate engulfment times and push-out distances, the maximum speeds of inward target movement (Fig. 4F) revealed an interesting similarity between the two types of phagocytosis. Considering targets of comparable size (zymosan particles and 3-µm Fc beads), our measurements yielded in both cases an average maximum target speed of ~33 nm/second. Remarkably, the target speed was conserved despite a significant difference in the cortical tension of the cells (Fig. 4G). The measured time courses of the cortical tension included in Fig. 4A,B demonstrate that during the uptake of zymosan particles, the tension typically rises higher, and remains elevated for a longer time, than during Fc-bead phagocytosis. The average maximum tension was ~0.3 mN/m for zymosan engulfment, whereas it only reached ~0.14 mN/m during the uptake of 3-µm Fc beads.

Finally, to verify that the ligand landscape presented by the target surface determined the type of mechanical cell response, we also examined the phagocytosis of zymosan particles that had been coated with rabbit polyclonal IgG antibodies. These ‘zymosan-Fc’ particles indeed elicited a neutrophil response that was intermediate between the cell behaviors observed with zymosan and Fc-beads (Fig. 4D–G). We note, however, that the averages included in Fig. 4D–G must be interpreted with caution. Our results exhibited a strong dependence on the time elapsed after the particles had been washed and suspended in the chamber buffer (which contained heat-treated serum but no IgG supplement), consistent with gradual depletion of IgG on the particle surface. For example, the maximum push-out distances of the cells tested at the beginning of this experiment were small, similar to the values obtained with Fc beads, but later they reverted to the large values characteristic for zymosan phagocytosis (supplementary material Fig. S1).

Effects of actin and myosin II inhibition

To explore whether the observed variations in phagocytic behavior can be related to key molecular players of cell motility, we repeated the above phagocytosis experiments in the presence of known inhibitors of actin polymerization (latrunculin A, cytochalasin D) and unconventional myosin II function (blebbistatin, ML-7, Y-27632; Fig. 6). Latrunculin sequesters actin monomers, and thus over time disrupts the cytoskeleton. Cytochalasin prevents F-actin polymerization. Blebbistatin is known to inhibit ATPases of non-muscle myosin II. ML-7 primarily inhibits the myosin light chain kinase, whereas Y-27632 suppresses activation of the myosin light chain through inhibition of Rho-associated protein kinases.

Our strategy was to fine-tune the inhibitor concentrations to values that produced a significant effect on at least one of the above observable parameters (control values of these parameters are shown in Fig 4D–G) but still allowed a reasonable fraction of tested neutrophils to complete phagocytosis. The chosen concentrations were: 50 µM blebbistatin, 10 µM ML-7, 10 µM Y-27632, 3 nM latrunculin and 500 nM cytochalasin, respectively. (Except for latrunculin, all concentrations were above the respective IC_{50} values.) The pre-incubation times of isolated neutrophils with these inhibitors (see Materials and Methods) were selected according to literature reports, although the actual timing of inhibition was longer due to the presence of drug in the experiment buffer.

We note that comparison of our inhibitor tests with traditional bulk studies requires caution, because any weakening of cell-target adhesion caused by an inhibitor will directly affect the statistics of phagocytosis in bulk assays, even if the cellular machinery governing engulfment is otherwise unaffected. By contrast, our dual-pipette manipulation system allows us to compensate for weaker adhesion by enforcing a longer or stronger contact between the cell and target. We were indeed able to establish cell adhesion to either target (zymosan particle or Fc bead) in the majority of single-cell experiments irrespective of the presence of inhibitors.

The main purpose of the inhibitor tests was to determine whether differences in the roles of actin polymerization or myosin II function could be detected between the two forms of phagocytosis. Because the degree to which an inhibitor affected the measurable quantities depended on dose, the most reliable criterion for such a difference would be an opposite trend in the effect of inhibitor. We note that due to the short lifespan of human neutrophils, only a few cells could be examined per blood draw, making these single-cell inhibition studies extremely tedious. Moreover, we often observed large variations in neutrophil behavior in the presence of inhibitors. Keeping these limitations in mind, we were unable to discern differential effects of the myosin II inhibitors on the two inspected forms of phagocytosis. Interestingly though, both actin inhibitors consistently produced the same, opposite, effects on the initial push-out phase of the two forms of phagocytosis. Whereas the presence of 3 nM latrunculin or 500 nM cytochalasin significantly decreased the push-out distance of zymosan, it produced an increase of this distance for Fc beads (Fig. 6B).

Common to all inhibitors were their effects on the maximum pull-in speed of both targets and on the cortical tension of neutrophils. The fastest pull-in speed remained largely unaffected under all tested conditions (Fig. 6C). By contrast, the maximum tension during phagocytosis was significantly lowered by all inhibitors (Fig. 6D).

In the remainder of this section we report noteworthy effects of individual inhibitors. Our experiments revealed a remarkable sensitivity of neutrophils to latrunculin. We found that phagocytosis (but not adhesion) of zymosan was completely impaired at latrunculin concentrations as low as 25 nM, which is much lower than latrunculin concentrations typically reported in the literature. We did occasionally observe a slight swelling of the cell local to the adherent target at a latrunculin concentration of 25 nM, but in no case did it lead to the formation of a pronounced pseudopod. On the other hand, zymosan was phagocytozed successfully in one out of six experiments performed at 10 nM latrunculin and in one out of three experiments at 5 nM of the drug, albeit on average slower than without the inhibitor. At 3 nM latrunculin, phagocytosis completed in about 70% of our single-cell experiments (averaged for both targets), and the primary drug effects in these experiments were, first, an, opposite effect on the target push-out distance in the two forms of phagocytosis (Fig. 6B) and second, a common decrease of the maximum cortical tension (Fig. 6D).

The literature on the effect of blebbistatin on human neutrophils is very sparse. We report that 50 μM (–)-blebbistatin decreased the cortical resting tension of quiescent neutrophils, measured in the absence of phagocytic targets as discussed previously (Lam et al., 2009), as well as the maximum tension during phagocytosis (Fig. 6D) by about one third compared to normal conditions. Other than that, we were surprised to find that blebbistatin did not significantly affect the engulfment of zymosan particles and antibody-coated beads by pipette-held human neutrophils (Fig. 6A–C). When manipulated into firm contact with a cell, both targets adhered to the neutrophil surface and phagocytosis appeared normal, even when we used concentrations as high as 400 μM of (±)-blebbistatin. We note, however, that the interpretation of blebbistatin effects requires caution, as evinced by microscopic inspection of cell suspensions incubated with the drug. Blebbistatin has a strong tendency to precipitate from buffers unless used within a day after suspension in aqueous solutions. In cases exhibiting such precipitation, the concentration of active blebbistatin is, of course, unknown. Another potential peril of using blebbistatin is its ambiguous specificity, as recently demonstrated by its effect on myosin-II-independent cellular processes (Shu et al., 2005).

The results obtained with the other myosin-II inhibitors were more ambiguous. The suppression of the initial target push-out by ML-7 (Fig. 6B) is unlikely to reflect a prominent role of myosin II in purely protrusive cell deformations. By contrast, the more direct myosin-II inhibitor blebbistatin had no effect on protrusion. Indeed, a recent study showed that ML-7 affects protrusion through non-specific inhibition of other kinases (Xu et al., 2008). Y-27632 decreased the maximum cortical tension of the neutrophils most strongly (which might be due to dose, as mentioned above), and otherwise seemed to produce intermediate effects between those of blebbistatin and ML-7.

Discussion

Phagocytosis rests on two key pillars: the biochemical recognition of pathogens, and an appropriate immunophysical response. Target recognition is generally based on specific receptor–ligand interactions. Positive identification of a particular target type may occur as late as in the phagosome, e.g. via interactions with toll-like receptors (Netea et al., 2007; Goodridge and Underhill, 2008; van de Veerdonk et al., 2008). On the other hand, the physical response of a cell to a pathogen must commence as early as possible for an efficient immune defense. One might expect, therefore, that all recognition scenarios share a common, early step that triggers a universal physical response program. Our single-cell experiments show that this is not so. Instead, zymosan phagocytosis follows a mechanistic route that is partially distinct from the uptake of antibody-coated targets.

The ability to resolve and quantify differences between the time-dependent mechanical behaviors of neutrophils during these two forms of phagocytosis is a key asset of our single-cell approach. However, other tasks such as the qualitative exploration of biochemical differences in target recognition are more efficiently pursued with assays that are not based on single-cell manipulation. Receptor–ligand interactions involved in the recognition of fungal and Fc targets, as well as target-specific signaling reactions, have been studied in the past using traditional bulk methods (Allen and Aderem, 1996; Herre et al., 2004; Swanson and Hoppe, 2004; Hall et al., 2006; Goodridge et al., 2009; van Bruggen et al., 2009). Even so, a clear picture of their relative physiological relevance and sequence of action has yet to be established. A synthesis of single-cell and bulk assays might ultimately be able, and perhaps required, to clarify the mechanistic details of target-specific recognition; however, such an undertaking is beyond the scope of this work.

We emphasize that we routinely added 10% heat-treated, autologous serum to the chamber buffer to mimic (to some extent) physiological conditions, and to prevent premature neutrophil activation upon cell contact with the glass surfaces of the bottom coverslip or the micropipette. Interestingly, when we added non-

heat-treated serum instead, all tested neutrophils recognized zymosan particles over a distance, i.e., without requiring physical contact. Mediated primarily by the chemoattractant C5a (produced by the complement system at the zymosan surface), this chemotactic recognition took the form of a neutrophil pseudopod growing toward the zymosan particle held a few micrometers away. Heat treatment of serum effectively suppressed this complement-mediated chemotaxis but not phagocytosis upon cell–target contact. In serum-free control experiments, plain zymosan particles almost never adhered to passive neutrophils even when forced into prolonged, strong contact using micropipettes. This shows that under our standard conditions, zymosan was opsonized with components of the (heat-treated) serum. We thus speculate that a mix of complement and antibody receptors, possibly in concert with specific receptors for the glycans on the zymosan surface, mediated the initial recognition of zymosan by passive neutrophils (Stuart and Ezekowitz, 2005; Goodridge et al., 2009; van Bruggen et al., 2009). The Fc targets, on the other hand, presumably were recognized by the neutrophil Fcγ receptors IIA (CD32A) and IIIB (CD16B), bearing in mind that constitutive expression of the high-affinity FcγRI (CD64) is minimal on quiescent human neutrophils (Bredius et al., 1994; Williams et al., 2000; Kakinoki et al., 2004; Selvaraj et al., 2004; Nimmerjahn and Ravetch, 2008).

Mechanical effectors of autonomous cell deformation

Before discussing the observed similarities and differences in terms of mechanics, we briefly review the set of mechanical effectors at the disposal of a cell. A simplified but instructive classification encompasses five categories: adhesion, protrusion, contraction, cortical tension and viscoelastic resistance to shape changes (Fig. 7). Adhesion provides bracing support during cell motion, enables phagocytes to hold on to their targets, and facilitates spreading of phagocytic cells over the target surface. The terms ‘protrusion’ and ‘contraction’ are used here as descriptors of outward and inward movement of parts of a motile cell, respectively. In both cases, the terminology could encompass a variety of underlying mechanisms. A prominent mechanism of autonomous cellular protrusion is the Brownian ratchet (Peskin et al., 1993). This is based on ever-present thermal fluctuations creating transient spaces required for the chemical addition of G-actin monomers to the growing ends of polymerizing F-actin. This polymerization causes asymmetry in the relative thermal motions of membrane and cytoskeleton, thus rectifying the fluctuations and generating a net repulsive force that drives protrusion.

‘Contraction’ is used here to describe any form of inward cell deformation that reduces the size of (part of) a cell. Examples of underlying mechanisms include pulling forces exerted by molecular motors, retrograde flow of cytoplasm, or enhanced crosslinking of cytoskeletal components.

The cortical tension resists surface-area expansion and maintains the spherical shape of passive cells in suspension. We also include in this category the mechanisms of recruitment of cell-surface area from various membrane reservoirs such as surface wrinkles or endovesicles (Herant et al., 2005; Hallett and Dewitt, 2007; Huynh et al., 2007).

Finally, the viscosities of the cytoplasm, nucleus and cell cortex determine the rate of cell deformation for a given set of mechanical driving forces. In particular, the speed of target inward movement is roughly set by the ratio between cortical tension and cytoplasmic viscosity (Tran-Son-Tay et al., 1991; Lam et al., 2009).

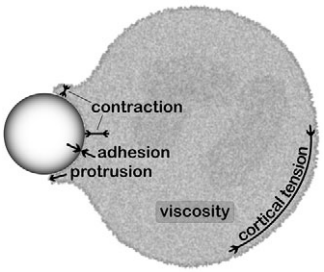

Fig. 7. Mechanical effectors of phagocytosis. Simplified categorization of distinct mechanical processes governing cellular motility, illustrating the limited ‘tool set’ at a cell’s disposal.

Protrusive zymosan phagocytosis versus enveloping uptake of Fc targets

The characteristic pedestal at the onset of zymosan engulfment is the most striking difference between the two phagocytosis forms. From a mechanical perspective, an initial outward push of a newly adherent target is not surprising. One of the first physical actions upon recognition of a pathogen is probably the generation of cellular protrusion in the proximity of the cell-surface patch in contact with the pertinent ligands. Therefore, one might generally expect that the first morphology change in any form of phagocytosis tends to push the target outwards, as observed with zymosan. Intriguingly, in antibody-mediated phagocytosis this ‘detour’ in cell morphology is suppressed, resulting in a much faster uptake of Fc targets. A strong correlation between push-out distance and target-engulfment time is indeed corroborated by our inhibitor tests.

The importance of actin polymerization in cell protrusion is confirmed not only by our confocal images in Fig. 3B, but also by the significant reduction of the initial zymosan push-out distance in our mild actin-inhibition tests (Fig. 6B). Surprisingly though, the same inhibitor concentrations produced an increase of this distance for Fc beads (Fig. 6B), suggesting that the actin cytoskeleton not only controls cell protrusion but also plays an important role in suppressing the outward displacement of phagocytic targets opsonized with antibodies. This dichotomous role of actin implies that structural interactions between the cytoskeleton and the membrane patch adherent to the target play a pivotal role in the mechanoregulation of the onset of target-specific phagocytosis.

A plausible mechanistic explanation of this behavior is based on a difference in strength of the structural anchoring complexes that link adherent membrane proteins to the cortical cytoskeleton in the two cases. Such linkages control to what extent transient spaces required for actin polymerization can form (cf. section on mechanical effectors), and they resist the protrusive force generated beneath the adherent membrane patch. Disruption of the cytoskeleton naturally acts to weaken these linkages, which explains the increase of the push-out distance of Fc targets if one assumes that the actin-dependent interaction between membrane and cytoskeleton is more sensitive to actin inhibition than the generation of protrusive force. Recent computer simulations have indeed provided strong support for this hypothesis (Herant et al., 2011).

Similar, but not identical, target internalization

Once zymosan particles are ‘pulled’ into the cell, their motion is similar to that observed during antibody-mediated phagocytosis

(Fig. 4F), suggesting an at least partially unified mechanistic program for the internalization of both target types. Even so, the different pseudopod morphologies indicate that the pathways never completely merge mechanistically. Instead, it appears that throughout the engulfment of zymosan, the neutrophil remains in a more 'alert' mode, continually probing the local environment for additional immunological stimuli.

Further disparity between the two types of phagocytosis is observed in the behavior of the cortical tension, particularly the larger maximum tension during the uptake of zymosan (Fig. 4G). Part of this difference can be explained by the concurrent disparity in pseudopod morphologies. The irregular and larger pseudopod enveloping a zymosan particle requires additional surface area (a crude estimate gave a maximum surface-area increase of 45±18% during zymosan phagocytosis; see supplementary material Fig. S2), which leads to a higher cortical tension (Herant et al., 2005; Hallett and Dewitt, 2007).

At a first glance, the tension difference (Fig. 4G) seems to be incompatible with the conserved pull-in speeds (Fig. 4F) of the two targets. The cortical tension is the main driver of target motion into the cell, as confirmed also by the synchronous onset of tension rise and target inward movement (cf. Fig. 4A,B). One would thus expect that higher tensions lead to faster target-pull-in speeds. By contrast, despite the twofold difference in maximum tensions, the target-internalization speeds are indistinguishable in the two cases. We reconcile this apparent contradiction by speculating that the cytoplasmic viscosity (the main mechanical effector of the rate of deformation) increases concurrently with tension. A higher viscosity will slow down cell deformation and thus countermand the tendency of the raised cortical tension to speed up target uptake. Further evidence for a strong correlation between cortical tension and cytoplasmic viscosity is provided by Fig. 6C,D, which reveals that despite a significant decrease of the cortical tension by all inhibitors, the target-internalization speed remains unchanged. This implies that these drugs lower tension and viscosity concurrently. Simultaneous reduction of the tension and viscosity has also been reported for neutrophils treated with cytochalasin B (Tsai et al., 1994). In agreement with the earlier demonstrated importance of a tight balance between tension and viscosity in eukaryotic cell motility (Lam et al., 2009), this strongly suggests that the cortical tension and the cytoplasmic viscosity are controlled by closely related molecular structures.

The involvement of F-actin in the maintenance of both tension and viscosity is not surprising; however, the role of myosin II is demonstrated here for the first time. Previous studies correlated decreased tensions with impairment of class I myosins in *Dictyostelium discoideum* (Dai et al., 1999; Schwarz et al., 2000) and in isolated organelles, intestinal epithelial cells, and fibroblasts (Nambiar et al., 2009).

Conclusions

Our ability to examine the time courses of controlled one-on-one interactions between phagocytes and their targets has exposed a wealth of new information. Validating our hypothesis that distinct forms of phagocytosis might involve different physical mechanisms, we have provided a quantitative side-by-side analysis of neutrophil phagocytosis of zymosan and antibody-coated particles. This comparison revealed that encounters of passive neutrophils with zymosan initially elicit a protrusive cell response that is not observed with Fc targets. The subsequent phagocytic uptake of zymosan appears to share some but not all of the cellular machinery employed by antibody-mediated phagocytosis. A brief summary of other important findings is: (1) Both actin and myosin II play a key role in the regulation of the cortical tension of neutrophils. The maximum tension during phagocytosis was significantly lowered by all used inhibitors. (2) The molecular structures that regulate the cortical tension and cytoplasmic viscosity of motile immune cells appear to be closely related (Lam et al., 2009). (3) Other than its effect on tension (and, presumably, viscosity), myosin II appears to play at most a minor role in phagocytic target internalization. (4) Actin, however, plays an intriguing dichotomous role in phagocytosis mechanics: it drives formation of a protrusive pseudopod that 'pushes' zymosan particles away at first, but also participates in the suppression of protrusion in the highly optimized uptake of antibody-coated targets. (5) We have established inhibitor concentrations that produce a significant effect on at least one of the quantifiable parameters characterizing phagocytosis, without blocking target uptake completely.

Compared to the swift phagocytosis of similarly sized Fc targets, the slower uptake of zymosan particles marks zymosan engulfment as the less efficient form of target internalization per se. One might speculate that evolutionary selection for the highest possible speed of target uptake has played a more important role in the optimization of antibody-mediated phagocytosis than in neutrophil interactions with zymosan (and, presumably, fungi in general). The mechanistic basis for the 2.5-fold faster uptake of Fc targets lies in the suppression of the initial outward displacement of these targets, which we attribute to stronger structural interactions between the cytoskeleton and the membrane patch in contact with the target.

Materials and Methods

Human neutrophils

Neutrophils were obtained from whole blood of healthy donors (informed consent was obtained from all subjects) in a total of about 100 draws (protocol approved by the Institutional Review Board, University of California Davis) (Herant et al., 2005).

Heparinized blood was underlaid with 5 ml PMN separation medium (Matrix/Thermo Fisher Scientific, Waltham, MA) and centrifuged at 700 ***g*** for 30 minutes to separate neutrophils from peripheral blood mononuclear cells. Isolated neutrophils were washed to remove remaining platelets (at 200 ***g*** for 10 minutes) in Hanks' balanced salt solution (HBSS without calcium or magnesium; Sigma-Aldrich, St Louis, MO) containing 0.1% human serum albumin (HSA; Gemini, Sacramento, CA), and then re-suspended in the same buffer but without HSA until use. For phagocytosis experiments, a small volume of this cell suspension was introduced into the experiment chamber containing HBSS with calcium and magnesium and 10% autologous serum that had been heat-treated (~60°C for 45 minutes). All single-cell experiments were carried out at room temperature.

For all inhibitor studies, the isolated neutrophils were pre-incubated at 37°C with the respective drug in test tubes that were continually rotated on a rolling apparatus (Stovall, Greensboro, NC) placed in an incubator. The pre-incubation times were as follows: 45 minutes for (–)-blebbistatin (Calbiochem, San Diego, CA); 30 minutes for latrunculin A (Calbiochem); 10 minutes for cytochalasin D (Calbiochem); 10 minutes for ML-7 (Sigma-Aldrich); and 15 minutes for Y-27632 (Calbiochem). Buffers used in phagocytosis experiments contained the same drug concentrations as used during pre-incubation. Except in the case of Y-27632, the pre-incubation and experiment buffers also contained 1% DMSO. Our inhibitor-free controls showed that at DMSO concentrations up to about 1%, the neutrophil behavior appeared normal. DMSO concentrations higher than 1%, however, altered cell morphology and/or behavior, and thus were not used in any phagocytosis experiments.

Phagocytosis targets

Zymosan particles (Sigma-Aldrich) were suspended in phosphate buffered saline (PBS; USB, Cleveland, OH) at 3-10 mg/ml, boiled in a water bath for 30 minutes, and stored at 4°C until use.

To coat zymosan particles with antibody, 1 µl of a 20 mg/ml particle suspension in PBS supplemented with 0.01% Tween 20 (PBST) was washed and incubated with 100 µl of zymosan-opsonizing reagent (derived from purified rabbit polyclonal IgG antibodies; Invitrogen) at 37°C for 1 hour. The particles were washed with PBST three times before introduction into the experiment chamber. We note that our protocol constituted a 100-fold increase of the vendor-recommended ratio (v/v) between zymosan-opsonizing reagent and zymosan particles; this increase was

necessary to achieve near-saturation of the zymosan surface with antibody (as verified by flow cytometry).

Polystyrene microspheres were opsonized with antibody as described (Herant et al., 2005). In short, beads with 3 or 5 μm nominal diameters (Duke Scientific/Thermo Fisher Scientific) were incubated overnight at 4°C in PBS containing 10 mg/ml bovine serum albumin (BSA; Sigma-Aldrich). After three washes in PBS without BSA, the beads were incubated at room temperature with rabbit polyclonal anti-BSA antibody (Sigma-Aldrich) for 1 hour. The beads were then washed three more times and re-suspended in PBS for storage at 4°C.

For phagocytosis experiments, a small volume of zymosan particles or antibody-coated beads were added to the experiment chamber filled with HBSS buffer (see neutrophil preparation above) that contained 10% heat-treated autologous serum.

Experiment chamber and micropipette manipulation

We have previously described micropipette manufacture and manipulation (Heinrich and Rawicz, 2005) as well as our dual-micropipette phagocytosis work stations (Herant et al., 2005) in detail. In short, micropipettes with an evenly broken, cylindrical tip of the desired inner diameter (here ~2–3 μm) were routinely produced before each experiment. Custom-written software interfaced a computer joystick with six motorized micrometers, allowing us to manipulate two pipettes in three dimensions. Automated application and measurement of pipette-suction pressure facilitated the gentle aspiration of neutrophils and phagocytosis targets. Together, this provided us with exquisite control over cell–target contacts away from the chamber bottom. Our software also allowed us to record video images and aspiration pressures at adjustable time intervals (at rates up to 30 full frames per second) to a computer hard disk. In addition, a separate, custom-written software application for image analysis greatly reduced manual tasks and human error when processing, at each time point, the target position relative to the pipette tip, the cell-projection length in the pipette, and the aspiration pressure.

To ensure quiescence of isolated neutrophils after their suspension in the chamber, we added 10% autologous serum to the experiment buffer, and we passivated the bottom coverslips by covalent attachment of 2-[methoxy (polyethyleneoxy) propyl] trichlorosilane (PEG-silane; Gelest, Morrisville, PA) as described earlier (Lam et al., 2009).

Measurement of the cortical tension and cell surface area

Assuming that the cortical tension γ of a passive, pipette-aspirated cell is uniform and isotropic (which is the case for fluid membranes), it can be expressed using Laplace's law in terms of the aspiration pressure Δp and the cell geometry (cf. supplementary material Fig. S2A) as $\gamma = \frac{1}{2}\,\Delta p R R_p/(R - R_p)$ (Heinrich and Rawicz, 2005; Herant et al., 2005). R is the radius of the spherical main cell body and R_p the pipette radius. For this formula to be valid, the condition $L_p \geq R_p$ must hold for the cell projection length inside the pipette, L_p. We also use this formula to estimate the cortical tension of irregularly shaped, active neutrophils during phagocytosis, inferring a representative value for R as follows in this case. The cell volume is measured initially for each resting, spherical neutrophil and is assumed constant throughout phagocytosis (which is a reasonable assumption as long as the buffer osmolarity remains constant). Measuring L_p at every time point during phagocytosis, we use the volume constraint to calculate the radius that the outer main cell body would have if it were a sphere, and we assign this value to R.

We estimate the neutrophil surface area during phagocytosis by approximating the irregular cell shape as a composite of spherical and cylindrical sections (cf. supplementary material Fig. S2B). The outer surface areas of these sections are summed to obtain the surface of the outer envelope of the deformed neutrophil. We also determine the cell–target contact area in an this manner (the zymosan surface is usually taken as the surface of an ellipsoid). The total cell surface area is the sum of the areas of the outer cell envelope and the membrane covering the target. We note that this estimation can only be used if the cell morphology remains nearly axisymmetric during target uptake, and even then it remains a crude approximation. More accurate contour tracking of pipette-held cells has been proposed (Liu et al., 2009); however, that method still relies on an axisymmetric configuration.

Scanning electron microscopy

Zymosan particles were seeded onto 12 mm (diameter) round coverslips in the same HBSS experiment buffer as described above. After 10 minutes, isolated neutrophils were added and allowed to interact with zymosan for 10 minutes. The specimens were washed twice in 0.1 M sodium phosphate buffer and fixed in Kronosky's fixing solution for 15 minutes. Following another two washes with 0.1 M sodium phosphate buffer, they were incubated in a series of 30%, 50% and 70% ethanol for 10 minutes each and washed twice in 95% and 100% ethanol for 5 minutes. The coverslips were twice incubated with hexamethyldisilazane (HMDS) for 10 minutes, and then dried. After sputter-coating (Pelco auto sputter coater SC-7; Ted Pella, Redding, CA), images were acquired on a Philips XL30 TMP scanning microscope (FEI, Hillsboro, OR) using analysis iTEM software.

Actin staining and confocal microscopy

A key goal of our immunofluorescence experiments was to image neutrophil–zymosan interactions in suspension. Neutrophils were incubated with fluorescent zymosan particles (Alexa Fluor 488 zymosan A conjugates; Invitrogen; reconstituted as recommended by Invitrogen) at a ratio of ~1:10 in the same buffer as used in our phagocytosis experiments (HBSS with calcium and magnesium and 10% heat-treated autologous serum). The cell–zymosan suspension was continually rotated on a Stovall roller at room temperature for 5 minutes.

The cells were then plated onto polylysine-coated glass coverslips that had been prepared as follows: Standard microscope coverslips (No. 1 thickness) were base-cleaned in a 1:1:5 mixture of ammonium hydroxide, 30% hydrogen peroxide, and water at boiling temperature for 10 minutes. After several washes in nanopure water, the coverslips were oven-dried, plasma-cleaned (Harrick Plasma, Ithaca, NY), soaked in a 10% aqueous solution of poly-L-lysine (Newcomer Supply/Thermo Fisher Scientific), and dried. The cell suspension was allowed to settle onto these coverslips for 5 minutes and then fixed with 0.2% glutaraldehyde in HBSS containing 50 mM MOPS (HBSS/MOPS, pH 7.2) for 10 minutes at room temperature. The now-adherent cells were washed and incubated with 0.05 M glycine (Sigma-Aldrich) in HBSS/MOPS at 4°C for 15 minutes to quench non-specific staining after fixation with glutaraldehyde.

Next, the cells were permeabilized with 0.01% Triton-X 100 (Sigma-Aldrich) and 3% BSA in PBS for 1 h. Actin staining was performed by incubating the samples with Alexa Fluor 488 phalloidin (1:200; Invitrogen) for 1 hour at room temperature.

Images were acquired with a Marianas system (Intelligent Imaging, Denver, CO) equipped with an AxioObserver microscope (Carl Zeiss MicroImaging, Thornwood, NY), a CoolSNAP HQ2 camera (Roper Scientific, Princeton Instruments, NJ), and a spinning disk confocal CSU10 system (Yokogawa, Newnan, GA). Image analysis was performed using Slidebook software (Intelligent Imaging, Denver, CO) and Adobe Photoshop (Adobe, San Jose, CA).

Statistical analysis

Significance of the differences of the mean values of data shown in Figs 4 and 6 was established by two-sample *t*-tests using Origin software (OriginLab, Northampton, MA). The *P*-values of all two-sample tests are given in supplementary material Table S1.

This work was supported by National Institutes of Health grant R01 A1072391. We are grateful to Soichiro Yamada for many discussions and his permission to use a spinning-disk confocal microscope. Scanning electron microscopy was carried out in the Electron Microscopy Laboratory of the Department of Medical Pathology and Laboratory Medicine (School of Medicine, University of California at Davis); we thank Patricia Kysar for instruction, and Jonathan Lam for his assistance in acquiring the images included in Fig. 3. We thank Chawin Ounkomol for preparing the sketch in Fig. 1A. Deposited in PMC for release after 12 months.

Supplementary material available online at
http://jcs.biologists.org/cgi/content/full/124/7/1106/DC1

References

Allen, L. A. and Aderem, A. (1996). Molecular definition of distinct cytoskeletal structures involved in complement- and Fc receptor-mediated phagocytosis in macrophages. *J. Exp. Med.* **184**, 627-637.

Araki, N. (2006). Role of microtubules and myosins in Fc gamma receptor-mediated phagocytosis. *Front. Biosci.* **11**, 1479-1490.

Bredius, R. G., Fijen, C. A., De Haas, M., Kuijper, E. J., Weening, R. S., Van de Winkel, J. G. and Out, T. A. (1994). Role of neutrophil Fc gamma RIIa (CD32) and Fc gamma RIIIb (CD16) polymorphic forms in phagocytosis of human IgG1- and IgG3-opsonized bacteria and erythrocytes. *Immunology* **83**, 624-630.

Dai, J., Ting-Beall, H. P., Hochmuth, R. M., Sheetz, M. P. and Titus, M. A. (1999). Myosin I contributes to the generation of resting cortical tension. *Biophys. J.* **77**, 1168-1176.

Dewitt, S. and Hallett, M. B. (2002). Cytosolic free Ca(2+) changes and calpain activation are required for beta integrin-accelerated phagocytosis by human neutrophils. *J. Cell Biol.* **159**, 181-189.

Di Carlo, F. J. and Fiore, J. V. (1958). On the composition of zymosan. *Science* **127**, 756-757.

Dormann, D., Weijer, G., Dowler, S. and Weijer, C. J. (2004). In vivo analysis of 3-phosphoinositide dynamics during Dictyostelium phagocytosis and chemotaxis. *J. Cell Sci.* **117**, 6497-6509.

Fletcher, D. A. and Mullins, D. (2010). Cell mechanics and the cytoskeleton. *Nature* **463**, 485-492.

Goodridge, H. S. and Underhill, D. M. (2008). Fungal recognition by TLR2 and Dectin-1. *Handb. Exp. Pharmacol.* **183**, 87-109.

Goodridge, H. S., Wolf, A. J. and Underhill, D. M. (2009). Beta-glucan recognition by the innate immune system. *Immunol. Rev.* **230**, 38-50.

Hall, A. B., Gakidis, M. A., Glogauer, M., Wilsbacher, J. L., Gao, S., Swat, W. and Brugge, J. S. (2006). Requirements for Vav guanine nucleotide exchange factors and Rho GTPases in FcgammaR- and complement-mediated phagocytosis. *Immunity* **24**, 305-316.

Hallett, M. B. and Dewitt, S. (2007). Ironing out the wrinkles of neutrophil phagocytosis. *Trends Cell Biol.* **17**, 209-214.
Hallett, M. B., von Ruhland, C. J. and Dewitt, S. (2008). Chemotaxis and the cell surface-area problem. *Nat. Rev. Mol. Cell Biol.* **9**, 662.
Heinrich, V. and Rawicz, W. (2005). Automated, high-resolution micropipet aspiration reveals new insight into the physical properties of fluid membranes. *Langmuir* **21**, 1962-1971.
Herant, M., Heinrich, V. and Dembo, M. (2005). Mechanics of neutrophil phagocytosis: behavior of the cortical tension. *J. Cell Sci.* **118**, 1789-1797.
Herant, M., Heinrich, V. and Dembo, M. (2006). Mechanics of neutrophil phagocytosis: experiments and quantitative models. *J. Cell Sci.* **119**, 1903-1913.
Herant, M., Lee, C.-Y., Dembo, M. and Heinrich, V. (2011). Protrusive push versus enveloping embrace: computational model of phagocytosis predicts key regulatory role of cytoskeletal membrane anchors. *PLoS Comput. Biol.* **7**, e1001068. doi:10.1371/journal.pcbi.1001068.
Herre, J., Marshall, A. S., Caron, E., Edwards, A. D., Williams, D. L., Schweighoffer, E., Tybulewicz, V., Reis, E., Sousa, C., Gordon, S. et al. (2004). Dectin-1 uses novel mechanisms for yeast phagocytosis in macrophages. *Blood* **104**, 4038-4045.
Holt, J. P., Bottomly, K. and Mooseker, M. S. (2007). Assessment of myosin II, Va, VI and VIIa loss of function on endocytosis and endocytic vesicle motility in bone marrow-derived dendritic cells. *Cell Motil. Cytoskeleton* **64**, 756-766.
Huynh, K. K., Kay, J. G., Stow, J. L. and Grinstein, S. (2007). Fusion, fission, and secretion during phagocytosis. *Physiology (Bethesda)* **22**, 366-372.
Janetopoulos, C., Ma, L., Devreotes, P. N. and Iglesias, P. A. (2004). Chemoattractant-induced phosphatidylinositol 3,4,5-trisphosphate accumulation is spatially amplified and adapts, independent of the actin cytoskeleton. *Proc. Natl. Acad. Sci. USA* **101**, 8951-8956.
Janeway, C. A., Jr and Medzhitov, R. (2002). Innate immune recognition. *Annu. Rev. Immunol.* **20**, 197-216.
Kakinoki, Y., Kubota, H. and Yamamoto, Y. (2004). CD64 surface expression on neutrophils and monocytes is significantly up-regulated after stimulation with granulocyte colony-stimulating factor during CHOP chemotherapy for patients with non-Hodgkin's lymphoma. *Int. J. Hematol.* **79**, 55-62.
Kaplan, G. (1977). Differences in the mode of phagocytosis with Fc and C3 receptors in macrophages. *Scand. J. Immunol.* **6**, 797-807.
Kay, R. R., Langridge, P., Traynor, D. and Hoeller, O. (2008). Changing directions in the study of chemotaxis. *Nat. Rev. Mol. Cell Biol.* **9**, 455-463.
Kobayashi, K., Inohara, N., Hernandez, L. D., Galan, J. E., Nunez, G., Janeway, C. A., Medzhitov, R. and Flavell, R. A. (2002). RICK/Rip2/CARDIAK mediates signalling for receptors of the innate and adaptive immune systems. *Nature* **416**, 194-199.
Lam, J., Herant, M., Dembo, M. and Heinrich, V. (2009). Baseline mechanical characterization of J774 macrophages. *Biophys. J.* **96**, 248-254.
Liu, X., Wang, Y. and Sun, Y. (2009). Cell contour tracking and data synchronization for real-time, high-accuracy micropipette aspiration. *IEEE Trans. Autom. Sci. Eng.* **6**, 536-543.
Medzhitov, R. and Janeway, C. A., Jr (2002). Decoding the patterns of self and nonself by the innate immune system. *Science* **296**, 298-300.
Nambiar, R., McConnell, R. E. and Tyska, M. J. (2009). Control of cell membrane tension by myosin-I. *Proc. Natl. Acad. Sci. USA* **106**, 11972-11977.
Netea, M., Meer, J. and Kullberg, B. (2007). Recognition of fungal pathogens by Toll-like receptors. In *Immunology of Fungal Infections* (ed. G. D. Brown and M. G. Netea), pp. 259-272. Netherlands: Springer.
Nimmerjahn, F. and Ravetch, J. V. (2008). Fc[gamma] receptors as regulators of immune responses. *Nat. Rev. Immunol.* **8**, 34-47.
Parent, C. A. and Devreotes, P. N. (1999). A cell's sense of direction. *Science* **284**, 765-770.
Patel, P. C. and Harrison, R. E. (2008). Membrane ruffles capture C3bi-opsonized particles in activated macrophages. *Mol. Biol. Cell* **19**, 4628-4639.
Peskin, C. S., Odell, G. M. and Oster, G. F. (1993). Cellular motions and thermal fluctuations: the Brownian ratchet. *Biophys. J.* **65**, 316-324.
Pillemer, L. and Ecker, E. E. (1941). Anticomplementary factor in fresh yeast. *J. Biol. Chem.* **137**, 139-142.
Schwarz, E. C., Neuhaus, E. M., Kistler, C., Henkel, A. W. and Soldati, T. (2000). Dictyostelium myosin IK is involved in the maintenance of cortical tension and affects motility and phagocytosis. *J. Cell Sci.* **113**, 621-633.
Selvaraj, P., Fifadara, N., Nagarajan, S., Cimino, A. and Wang, G. (2004). Functional regulation of human neutrophil Fc γ receptors. *Immunol. Res.* **29**, 219-229.
Shu, S., Liu, X. and Korn, E. D. (2005). Blebbistatin and blebbistatin-inactivated myosin II inhibit myosin II-independent processes in Dictyostelium. *Proc. Natl. Acad. Sci. USA* **102**, 1472-1477.
Stuart, L. M. and Ezekowitz, R. A. (2005). Phagocytosis: elegant complexity. *Immunity* **22**, 539-550.
Swanson, J. A. (2008). Shaping cups into phagosomes and macropinosomes. *Nat. Rev. Mol. Cell Biol.* **9**, 639-649.
Swanson, J. A. and Hoppe, A. D. (2004). The coordination of signaling during Fc receptor-mediated phagocytosis. *J. Leukoc. Biol.* **76**, 1093-1103.
Touret, N., Paroutis, P., Terebiznik, M., Harrison, R. E., Trombetta, S., Pypaert, M., Chow, A., Jiang, A., Shaw, J., Yip, C. et al. (2005). Quantitative and dynamic assessment of the contribution of the ER to phagosome formation. *Cell* **123**, 157-170.
Tran-Son-Tay, R., Needham, D., Yeung, A. and Hochmuth, R. M. (1991). Time-dependent recovery of passive neutrophils after large deformation. *Biophys. J.* **60**, 856-866.
Tsai, M. A., Frank, R. S. and Waugh, R. E. (1994). Passive mechanical behavior of human neutrophils: effect of cytochalasin B. *Biophys. J.* **66**, 2166-2172.
Underhill, D. M. and Ozinsky, A. (2002). Phagocytosis of microbes: complexity in action. *Annu. Rev. Immunol.* **20**, 825-852.
van Bruggen, R., Drewniak, A., Jansen, M., van Houdt, M., Roos, D., Chapel, H., Verhoeven, A. J. and Kuijpers, T. W. (2009). Complement receptor 3, not Dectin-1, is the major receptor on human neutrophils for beta-glucan-bearing particles. *Mol. Immunol.* **47**, 575-581.
van de Veerdonk, F. L., Kullberg, B. J., van der Meer, J. W. M., Gow, N. A. R. and Netea, M. G. (2008). Host-microbe interactions: innate pattern recognition of fungal pathogens. *Curr. Opin. Microbiol.* **11**, 305-312.
Williams, T. E., Nagarajan, S., Selvaraj, P. and Zhu, C. (2000). Concurrent and independent binding of Fcgamma receptors IIa and IIIb to surface-bound IgG. *Biophys. J.* **79**, 1867-1875.
Xu, J., Gao, X. P., Ramchandran, R., Zhao, Y. Y., Vogel, S. M. and Malik, A. B. (2008). Nonmuscle myosin light-chain kinase mediates neutrophil transmigration in sepsis-induced lung inflammation by activating beta2 integrins. *Nat. Immunol.* **9**, 880-886.